Journal of Alloys and Compounds 693 (2017) 565–572

Contents lists available at ScienceDirect

Journal of Alloys and Compounds

journal homepage: http://www.elsevier.com/locate/jalcom

Role of ion species in radiation effects of $Lu_2Ti_2O_7$ pyrochlore

Dongyan Yang [a, b], Yue Xia [a], Juan Wen [a], Jinjie Liang [a, b], Pengcheng Mu [a], Zhiguang Wang [b], Yuhong Li [a, *], Yongqiang Wang [c]

[a] School of Nuclear Science and Technology, Lanzhou University, Lanzhou 730000, China
[b] Institute of Modern Physics, Chinese Academy of Sciences, Lanzhou 730000, China
[c] Materials Science and Technology Division, Los Alamos National Laboratory, Los Alamos, NM 87545, USA

ARTICLE INFO

Article history:
Received 16 July 2016
Received in revised form
12 September 2016
Accepted 20 September 2016
Available online 21 September 2016

Keywords:
Radiation effects
Ion species
Pyrochlores
Amorphization
Lattice swelling

ABSTRACT

In an attempt to investigate the role of ion species in the radiation effects of pyrochlores, polycrystalline $Lu_2Ti_2O_7$ samples, prepared through a standard solid state process, were irradiated with three different ion beams: 400 keV Ne^{2+}, 2.7 MeV Ar^{11+} and 6.5 MeV Xe^{26+}. To characterize the damaged layers in $Lu_2Ti_2O_7$, the grazing incident X-ray diffraction technique was applied. All the three irradiations induce significant amorphization processes and lattice swelling in $Lu_2Ti_2O_7$. However, when the ion fluence is converted to a standard dose in dpa, the radiation effects of $Lu_2Ti_2O_7$ show a great dependence on the implanted ion species. The threshold amorphization dose decreases with increasing ion mass and energy. Besides, the amorphization rate, as well as lattice swelling rate, increases with increasing ion mass and energy. That is, the $Lu_2Ti_2O_7$ pyrochlore is more susceptible to amorphization and lattice swelling under heavier ion irradiation. These results are then discussed in the framework of defect configuration and the density of collision cascades based on Monte Carlo simulations.

1. Introduction

Global expansion of nuclear power has been proposed as an excellent solution to the problems associated with increasing energy use, excessive dependence on fossil fuels and greenhouse gas emissions [1–4]. However, the management of increasing radioactive wastes becomes one of the important concerns in the development of nuclear power. The safe immobilization of toxic nuclear wastes, including minor actinides (U, Np, Th, Am and Cm) in spent nuclear fuel and Pu from dismantled nuclear weapons, is a major challenge facing humanity today. Currently, ceramic materials, which can survive in the extreme environment of radiation, are proposed as potential matrices for the disposal of high-level radioactive wastes [3–6].

The pyrochlores with formula of $A_2B_2O_7$ (A = Rare earths, B = Zr, Ti, Sn and Hf) are promising ceramic host phases for the immobilization of actinides [7–9]. $A_2B_2O_7$ pyrochlores belong to $Fd\bar{3}\ m$ space group, and have a superstructure of the well-known fluorite structure ($Fm\bar{3}\ m$). The unit cell contains eight molecules (Z = 8) and four crystallographically nonequivalent sites. As the origin is fixed on B site, atoms occupy the following special positions: A at 16*d* (0.5, 0.5, 0.5), B at 16*c* (0, 0, 0), O at 48*f* (*x*, 0.125, 0.125) and 8*b* (0.375, 0.375, 0.375). The 8*a* site is unoccupied. Among these coordinates, only the 48*f* oxygen position parameter (*x*) is changeable. Both the cations and the anion vacancies are ordered on the cation and anion sublattice respectively, and the pyrochlore can be regarded as an ordered defective fluorite structure.

Extensive studies have been devoted to the radiation effects of titanate and zirconate pyrochlores irradiated with various ion beams [9–23]. Pyrochlores generally undergo significant structural evolution under ion irradiations, including amorphization [10,17], order-to-disorder phase transformation [24], lattice swelling [12,25,26] and phase separation [12]. The factors that govern the radiation tolerance of pyrochlores are quite complex, mainly involving the 48*f* oxygen positional parameter (*x*) [10], the radius ratio of A- to B-cation [21–23], the defect energetics [27–30], the ionicity of chemical bonds [14,31], the formation enthalpy [32], as well as the inherent atomic disorder [13,18]. First principles calculations have shown that the cation antisite defect is the most energetically favorable defect in $Sm_2Ti_2O_7$, $Gd_2Ti_2O_7$ and $Lu_2Ti_2O_7$ pyrochlores [25,29]. However, a molecular dynamics simulation investigation [33] shows that it is the cation Frenkel pair defect rather than the cation antisite defect that contributes to the amorphization in $Gd_2Ti_2O_7$ [10].

* Corresponding author.
E-mail address: liyuhong@lzu.edu.cn (Y. Li).

http://dx.doi.org/10.1016/j.jallcom.2016.09.227
0925-8388/

From the perspective of implanted ions, the mass and energy are critical factors which determine the energy deposition of the ions and thereby the damage build-up in target materials [34,35]. The effects of ion species have been mentioned in various experimental studies [9,36], including materials such as $Cd_2Nb_2O_7$, $Gd_2Ti_2O_7$, $Lu_2Ti_2O_7$, $Ca_2La_8(SiO_4)_6O_2$ and 6H-SiC, where the efforts were mainly focused on the critical amorphization temperatures and recovery activation energies. However, the discrepancy of radiation effects of materials under different ion irradiations was not well understood yet, which correlates the results of ion beam irradiation experiments to the radiation damage induced by α- and β-events in nuclear waste matrices. Herein, we report on a systematic study of the influence of ion species (400 keV Ne^{2+}, 2.7 MeV Ar^{11+} and 6.5 MeV Xe^{26+}) on the radiation behavior of $Lu_2Ti_2O_7$.

2. Experimental details

Polycrystalline $Lu_2Ti_2O_7$ samples were prepared via a standard solid state process. Stoichiometric amounts of Lu_2O_3 (99.99% pure) and TiO_2 (99.99% pure) were intimately mixed using a ball-mill. The powders were subsequently pressed into pellets at the pressure of ~400 MPa. The compacts were first sintered at 1200 °C for 24 h. To attain better homogeneity, the procedures (grinding, milling and pressing) were repeated with a second heating at 1450 °C for 48 h. The resulted pellets were then polished to a mirror finish.

$Lu_2Ti_2O_7$ samples were irradiated with three ion species with different masses and energies. The 400 keV Ne^{2+} ion irradiations were carried out at cryogenic temperature (~77 K) using a 200 kV Danfysik high current research ion implanter in the Ion Beam Materials Laboratory at Los Alamos National Laboratory, and the 2.7 MeV Ar^{11+} and 6.5 MeV Xe^{26+} ion irradiations were performed at room temperature (~293 K) on a 320 kV platform for multi-discipline research with highly charged ions at the Institute of Modern Physics, Chinese Academy of Sciences (CAS). All the ions were implanted at normal incidence. The ion fluences for different irradiations are listed in Table 1. The flux of each ion irradiation is significantly low ($\leq 1 \times 10^{12}$ ions/(cm^2·s)), and thus the flux effect was neglected in the following discussion section.

To estimate the ranges, energy deposition and displacement damages of each ion irradiation, the ion transport Monte Carlo simulations were performed using the SRIM (Stopping and Range of Ions in Matter) code with the Full Damage Cascades mode [37]. In these simulations, the threshold displacement energies for Lu, Ti and O atom were set as 84, 205 and 52 eV respectively, as calculated for $Gd_2Ti_2O_7$ pyrochlore [38]. The ion projected range of 400 keV Ne ions is ~0.40 μm, which is much smaller than those of 2.7 MeV Ar and 6.5 MeV Xe ion (1.19 and 1.25 μm respectively). Fig. 1 shows the variation of displacement damage as a function of depth under each irradiation at the fluence of 1×10^{15} ions/cm^2. The maximum peak displacement damages at fluence of 1×10^{15} ions/cm^2 are approximately 0.20, 0.35 and 1.39 dpa (displacements per atom) for Ne, Ar and Xe irradiation respectively. According to this result, the ion fluence (in ions/cm^2) of each irradiation was converted into a standard damage dose (in dpa) for ease of comparison among different ion species, as presented in Table 1. Table 1 also gives the ion projected range (R_p), as well as the nuclear (S_n) and electronic (S_e) energy loss.

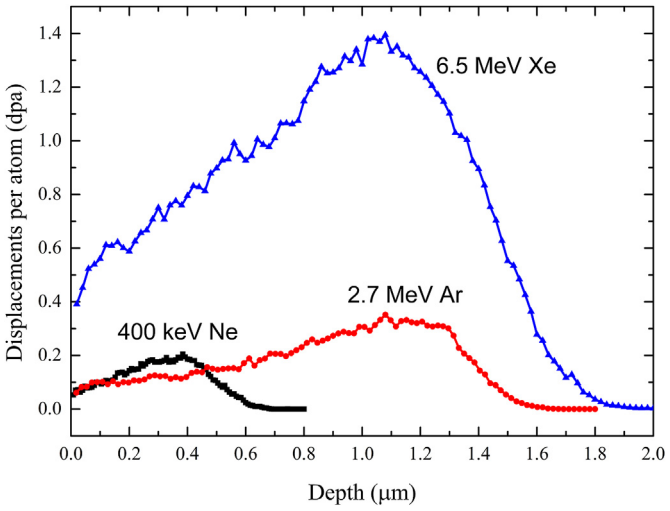

Fig. 1. Variation of the displacement damage vs. depth in $Lu_2Ti_2O_7$ for 400 keV Ne, 2.7 MeV Ar and 6.5 MeV Xe ion implantations at fluence of 1.0×10^{15} ions/cm^2.

Ion irradiation induced structural damage was characterized by grazing incident X-ray diffraction (GIXRD) method. For $Lu_2Ti_2O_7$ samples irradiated with 400 keV Ne^{2+} ions, please see Ref. [25]. For $Lu_2Ti_2O_7$ samples irradiated with 2.7 MeV Ar^{11+} and 6.5 MeV Xe^{26+} ions, the X-ray incidence angle was $\gamma = 1°$. The scan range of 2θ is from 10° to 70°, with a step of 0.02° and a dwell time of 1 s. The incident angles chosen here can ensure that only radiation damaged layers were detected by X-rays.

3. Results

Fig. 2 displays the normalized GIXRD patterns of $Lu_2Ti_2O_7$ samples before and after 400 keV Ne^{2+} (a), 2.7 MeV Ar^{11+} (b) and 6.5 MeV Xe^{26+} (c) irradiations, illustrating the structural evolution with increasing ion dose. For the pristine $Lu_2Ti_2O_7$ (see the bottom pattern in Fig. 2(a)), each diffraction peak can be referred to the pyrochlores structure, as labeled with the Miller indices. Actually two series of diffraction peaks are observed. The first series with high intensities contains the peaks corresponding to the parent fluorite structure, as marked with even Miller indices (such as (2 2 2), (4 0 0) and (4 4 0)). The second series with low intensities, as marked with odd Miller indices (such as (1 1 1), (3 1 1) and (3 3 1)), corresponds to the superstructure of the ordered $A_2B_2O_7$ pyrochlore. The XRD pattern reveals that pristine $Lu_2Ti_2O_7$ samples

Table 1
The irradiation parameters for each irradiation on $Lu_2Ti_2O_7$.

Ion species	R_p (μm)	S_n[a]	S_e[a]	Irradiation fluences and doses					
		keV/nm							
400 keV Ne^{2+}	0.40	0.15	0.68	Fluence (ions/cm^2)	0	7×10^{14}	1×10^{15}	2×10^{15}	4×10^{15}
				Dose (dpa)	0	0.14	0.20	0.40	0.80
2.7 MeV Ar^{11+}	1.19	0.22	1.88	Fluence (ions/cm^2)	0	2×10^{14}	4×10^{14}	6×10^{14}	8×10^{14}
				Dose (dpa)	0	0.07	0.14	0.21	0.28
6.5 MeV Xe^{26+}	1.25	1.20	3.45	Fluence (ions/cm^2)	0	2×10^{13}	3.5×10^{13}	5×10^{13}	1.2×10^{14}
				Dose (dpa)	0	0.03	0.05	0.07	0.17

[a] The mean values of nuclear and electronic energy loss within the range from the implanting surface to the depth of displacement damage peak.

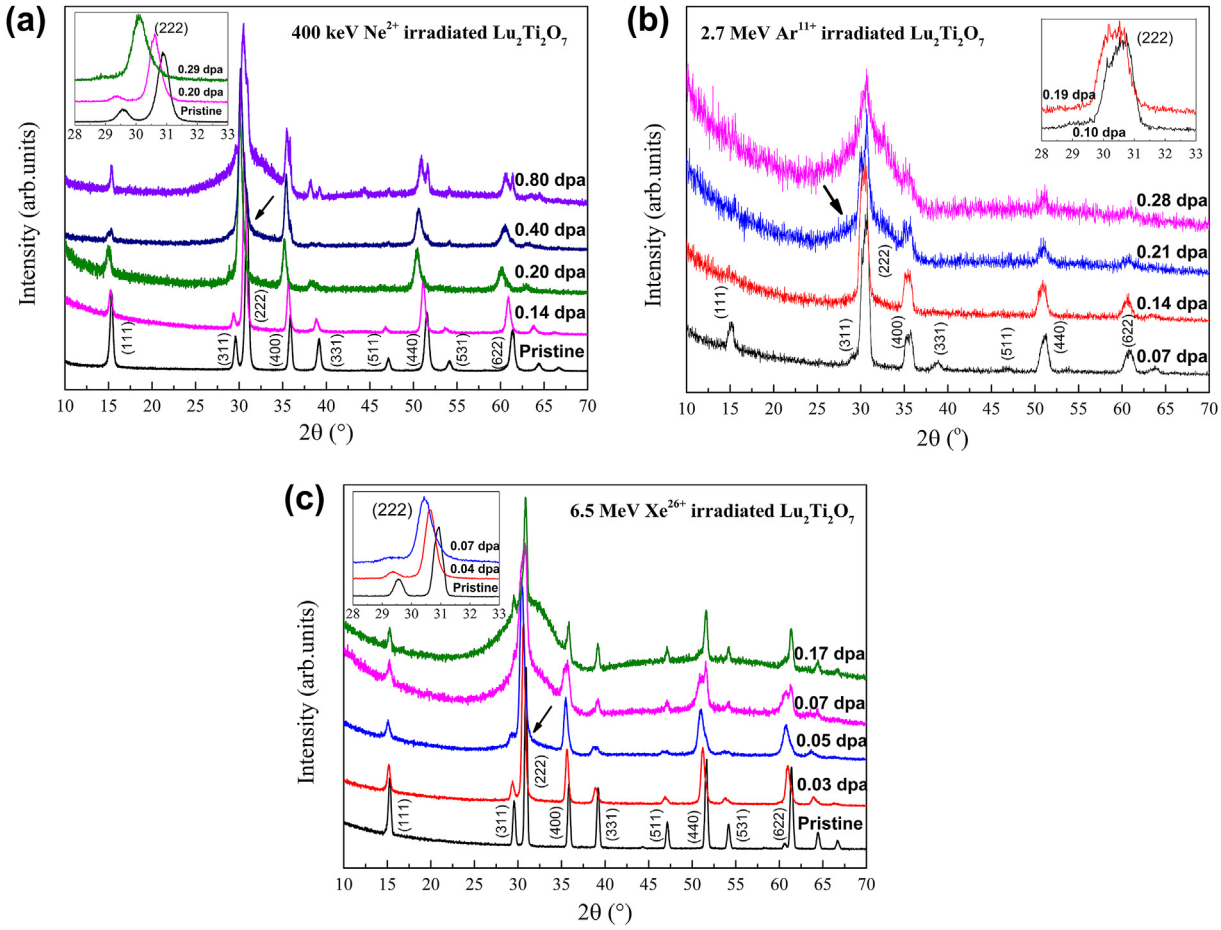

Fig. 2. GIXRD patterns of $Lu_2Ti_2O_7$ under three ion irradiations: (a) 400 keV Ne^{2+}, (b) 2.7 MeV Ar^{11+} and (c) 6.5 MeV Xe^{26+}. The diffraction peaks are marked with the corresponding Miller indices. The arrows indicate the diffuse scattering from amorphization domains. The insets are enlarged views of the range $2\theta = 28°–33°$ to show the peak shift with increasing irradiation dose.

possess an ideal pyrochlore structure.

400 keV Ne^{2+} ion irradiation induced structural evolution is clearly indicated in Fig. 2(a). With increasing irradiation dose, the first striking observation is the diminished intensity of odd diffraction peaks. As the dose reaches 0.40 dpa, the superlattice diffraction peaks almost vanish, except that only (1 1 1) peak is still visible. As mentioned above, these odd reflections are characteristics of the pyrochlore superstructure, which are related to the ordered arrangement of A- and B- cations on the cation sublattice. The decreased intensity means that an order-to-disorder (O-D) phase transition is induced by 400 keV Ne^{2+} ion irradiation. Another phenomenon is the irradiation induced amorphization. At dose of 0.40 dpa, slight diffuse scattering occurs at the basis of the most intense peak (2 2 2), which arises from an amorphous phase. Finally, at the highest dose of 0.80 dpa, the amorphization becomes much more significant, implying that a crystalline-to-amorphization phase transformation is induced by 400 keV Ne^{2+} irradiation. Before amorphization occurs (at doses below 0.40 dpa), all the diffraction peaks shift to lower 2θ with increasing dose. The inset in the upper left corner is an enlarged view of $2\theta = 28°–33°$, which clearly shows the shift of (2 2 2) peak. Based on the Bragg equation,

$$2dsin\theta = n\lambda, \tag{1}$$

and the correlation between the lattice parameter (a) and interplanar spacing (d) for cubic crystals,

$$a = d\sqrt{h^2 + k^2 + l^2}, \tag{2}$$

this shift indicates the lattice parameter of $Lu_2Ti_2O_7$ is increased under irradiation before amorphization. In other words, a lattice swelling effect is induced in $Lu_2Ti_2O_7$ by 400 keV Ne^{2+} irradiation [25].

Fig. 2(b) presents the typical GIXRD patterns of $Lu_2Ti_2O_7$ under 2.7 MeV Ar^{11+} ion irradiation with increasing dose. It is clear that all the pyrochlore superlattice diffraction peaks, such as (1 1 1), (3 1 1) and (3 3 1), vanish at dose of 0.14 dpa, indicating a complete order-to-disorder phase transition is achieved in $Lu_2Ti_2O_7$ under Ar^{11+} irradiation. Strong diffuse scattering is observed at the basis of (2 2 2) peak at 0.21 dpa, which means that $Lu_2Ti_2O_7$ is severely amorphized by 2.7 MeV Ar^{11+} ion irradiation at this dose. As the dose increases to 0.28 dpa, the amorphous state is enhanced further. Besides, as shown in the inset, the (2 2 2) peak shifts to lower 2θ with increasing dose, indicating that the lattice swelling effect is also observed under Ar^{11+} irradiation.

For the 6.5 MeV Xe^{26+} ions irradiated $Lu_2Ti_2O_7$, the GIXRD patterns are presented in Fig. 2(c). $Lu_2Ti_2O_7$ samples under Xe^{26+} irradiations undergo structural evolution similar with the above two cases. As shown in Fig. 2(c), under low dose (≤0.05 dpa) irradiations, the intensity of pyrochlore superlattice peaks decreases with increasing dose and all diffraction peaks shift to lower 2θ (as shown in the inset), implying that both O-D transition and lattice swelling

are induced by Xe^{26+} irradiations. At dose of 0.05 dpa, slight diffuse scattering occurs at the basis of (2 2 2) peak, which is an evidence of the amorphous phase. As the irradiation dose increases to 0.17 dpa, $Lu_2Ti_2O_7$ sample is severely amorphized, where another broad diffuse scattering band is also examined at 2θ range from 40° to 60°.

Based on the experimental results above, similar structural evolution was found in $Lu_2Ti_2O_7$ pyrochlore under three different ion species irradiations: 400 keV Ne^{2+}, 2.7 MeV Ar^{11+} and 6.5 MeV Xe^{26+}. The samples undergo O-D phase transformation, lattice swelling and amorphization. However, the threshold amorphization doses (the dose at the onset of amorphization process) for the three ion irradiations are significantly different, suggesting that the amorphization mechanism would be closely associated with the nature of implanted ions.

4. Discussion

4.1. Effect of ion species on amorphization and lattice swelling

For a more detailed perspective of the effect of ion species on the amorphization processes in $Lu_2Ti_2O_7$, a quantitative analysis of amorphous fraction with increasing irradiation dose was performed. Based on the method in Ref. [23], the fraction of amorphous phase was extracted using a peak-fitting procedure of XRD patterns. As illustrated in Fig. 3, the XRD pattern can be decomposed into four different contributions consisting of a diffuse broad peak (marked as *a*) from the amorphous part of samples and three crystalline peaks (marked as *b*, *c* and *d*). Pseudo-Voigt profiles were used to fit these peaks. The amorphous fraction (f_a) was deduced from the ratio of the amorphous-peak area (S_a, the shaded area in Fig. 3) to the total peak area ($S_a + S_b + S_c + S_d$),

$$f_a = \frac{S_a}{S_a + S_b + S_c + S_d} \tag{3}$$

According to the method above, the amorphous fraction in $Lu_2Ti_2O_7$ as a function of dose for each ion irradiation was calculated and plotted in Fig. 4. The amorphous fraction increases with different rates and functions with respect to irradiation dose for different ion species. From Fig. 4(a), it can be seen that the amorphous domain occurs at dose > 0.20 dpa, and then the amorphous fraction increases systematically as an function of irradiation dose to ~8.41% at dose of 0.40 dpa and finally ~66.38% at 0.80 dpa. Based on the previously proposed amorphization mechanisms [39], this behavior of amorphization fraction with increasing dose can be ascribed to a defect-accumulation-like amorphization model, where the amorphization phase forms when the local defect density reaches a threshold level during the defect accumulation process due to the overlapping of collision cascades. Fig. 4(b) shows the variation of amorphous fraction with increasing dose under 2.7 MeV Ar^{11+} ion irradiation. The sigmoidal-like growth of amorphous fraction can be well described with a direct-impact/defect-stimulated (DI/DS) model. This model assumes that the amorphization occurs from both direct-impact (in-cascade) production and defect-stimulated production. According to the fitting results, the cross section of defect-stimulated amorphization is estimated to be 25.37 dpa^{-1}, which is much larger than that of direct-impact induced amorphization (0.23 dpa^{-1}). Therefore, it is clear that for the energy regime of 2.7 MeV Ar^{11+} ions irradiation, the probability of direct amorphization is relatively low, while the defect-stimulated amorphization is the dominant mechanism for the damage accumulation in $Lu_2Ti_2O_7$. See Ref. [40] for more details. For 6.5 MeV Xe^{26+} irradiated samples, the amorphous fraction as a function of irradiation dose is plotted in Fig. 4(c). One can see that, at very low dose (≤0.03 dpa) irradiation, no amorphization was detected. As the dose continues increasing, the amorphous fraction grows dramatically. Although this variation trend is similar to that of 2.7 MeV Ar^{11+} irradiation, the DI/DS model was failed to fit the result in Fig. 4(c). If we ignore the data at dose of 0 and 0.03 dpa, the *Amorphous fraction-Dose* curve is quite similar with the well-established direct-impact model in other systems irradiated with heavy ion irradiations [21,23,41,42]. Based on the direct-impact model, a highly energetic incident ion transfers its kinetic energy to the target system within 10^{-13} s, and creates a dense displacement cascade. The highly energetic zone quenches quickly (within a few ps) to form an amorphous domain. Therefore, it is reasonable to accept that direct-impact induced amorphization would play a predominant role in the damage build-up of $Lu_2Ti_2O_7$ under 6.5 MeV Xe^{26+} irradiation.

In order to facilitate an intuitive comparison, the *Amorphization fraction-Dose* curves for all ion irradiations were merged into one graph, as shown in Fig. 4(d). It is apparent that the threshold amorphization dose decreases with increasing mass and energy of implanted ions. And with respect to the same amorphization fraction, the dose required for heavier Ar^{11+} and Xe^{26+} ions are evidently lower as compared with Ne^{2+} ion. It should be noted that, in our study, Ne^{2+} irradiations were performed at cryogenic temperature (~77 K), and Ar^{11+} and Xe^{26+} irradiations were performed at room temperature (~293 K). Our recent study [43] has demonstrated that the amorphization dose of $Lu_2Ti_2O_7$ is a constant at low irradiation temperature range (0–400 K), and increases rapidly with increasing temperature at high temperature range (>400 K), which is also confirmed by *Lian*'s results [10]. Therefore, if the Ne^{2+} irradiations were carried out at room temperature (same with the Ar^{11+} and Xe^{26+} cases) on $Lu_2Ti_2O_7$, the threshold amorphization dose would be equal to (or maybe greater than) that obtained in present cryogenic case. Thus, the conclusion that the threshold dose for amorphization decreases with increasing mass and energy of irradiation ions is unquestionable. In other words, the heavier ions are more efficient to induce amorphization in $Lu_2Ti_2O_7$. Since the dose in dpa is a standard estimation for the ion irradiation induced displacement damage, the same dose means that the same amount of displacement events were produced. Evidently, as demonstrated in the present study, the same amount of

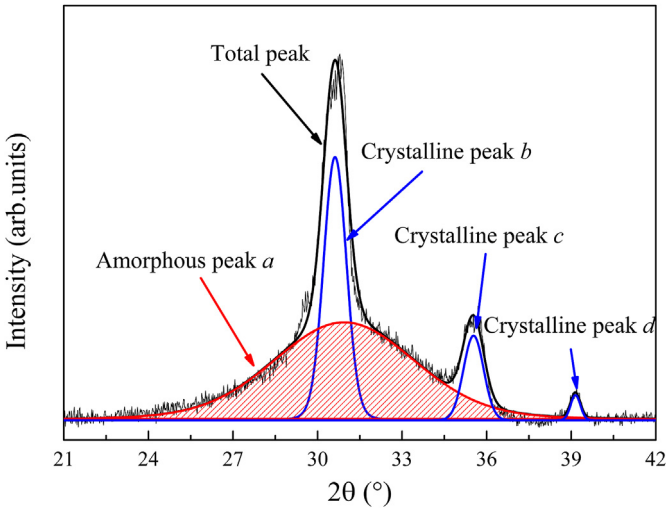

Fig. 3. The schematic diagram of peak-fitting analysis of GIXRD pattern (of $Lu_2Ti_2O_7$ under 6.5 MeV Xe^{26+} irradiation at 0.07 dpa) for amorphous fraction calculation. The pattern can be decomposed into four different contributions of three crystalline peaks (*b*, *c* and *d*) and a broad amorphous peak (*a*, the shaded area). Pseudo-Voigt profiles are used to fit these individual peaks. The amorphous fraction is determined by the peak-area ratio $S_a/(S_a + S_b + S_c + S_d)$.

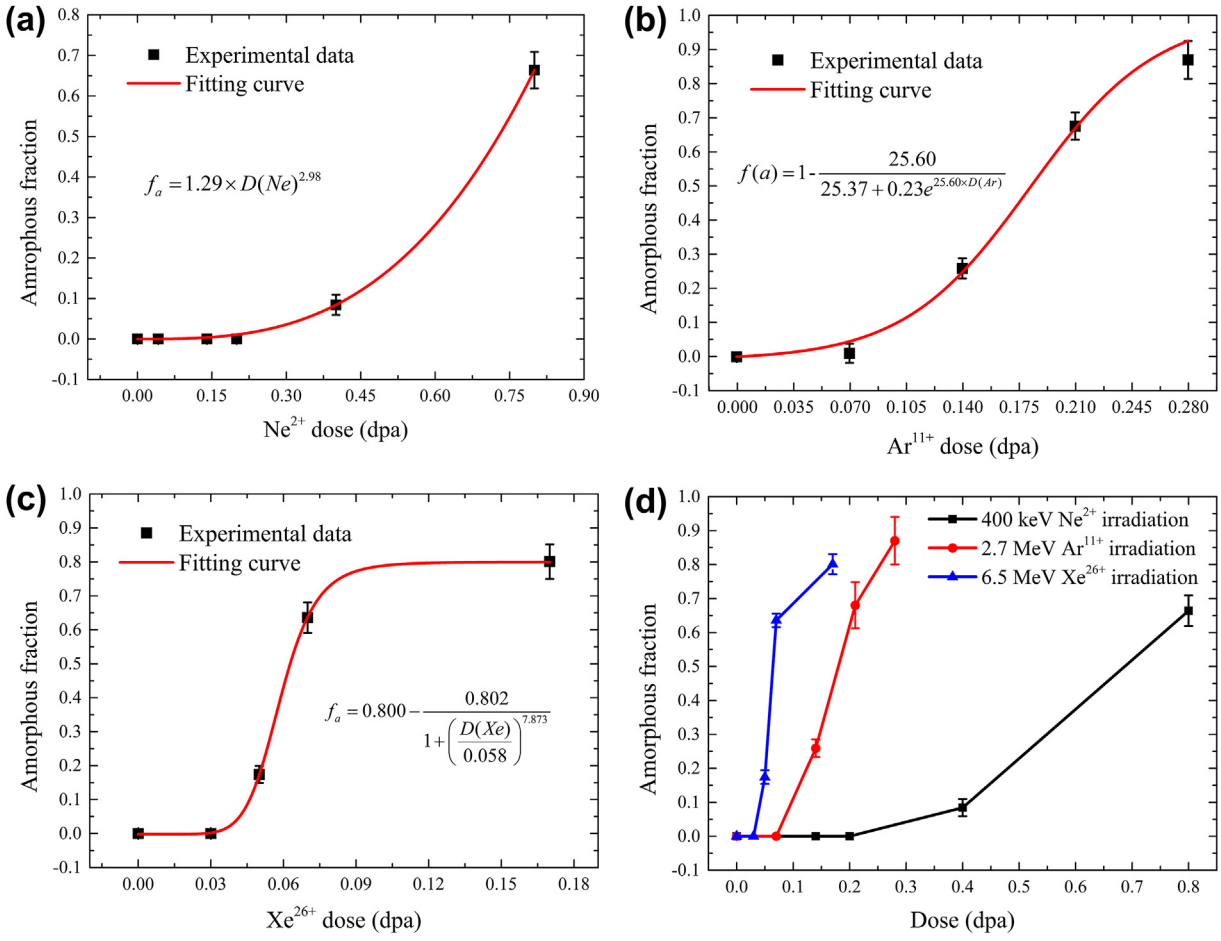

Fig. 4. The amorphous fraction as a function of irradiation dose for (a) 400 keV Ne^{2+}, (b) 2.7 MeV Ar^{11+} [40] and (c) 6.5 MeV Xe^{26+} ion irradiations. (d) is a merged view of (a), (b) and (c) to facilitate an intuitive comparison. The black points in (a), (b) and (c) are experimental data and the red lines are fits to the data.

displacement events evolved into amorphization damages of different extents in $Lu_2Ti_2O_7$ under different ion species irradiations. The similar dependence of amorphization dose on irradiation ion mass was also reported in other systems [9,36], where the amorphization dose decreases with increasing ion mass. However, there exists an opposite example, i.e., the amorphization dose of zircon increases with increasing ion mass (Kr, Xe, Bi and U ion irradiations) at temperature range from 20 to 400 K [44].

In Fig. 4(c), it is clear that the fraction of amorphous phase saturates at about 80%, which suggests a recovery effect at room temperature. This result agrees very well with a recently published work by *Rong* [42], where the amorphization fraction in $Lu_2Ti_2O_7$ also saturates at ~80% under 600 keV Kr^{3+} ion irradiation. Since the Ne^{2+} irradiations were done at cryogenic temperature, the defects are "frozen" once formed and the recovery is extremely inhibited. A full amorphous state is expected in $Lu_2Ti_2O_7$ due to the continuous accumulation of defects. As for the Ar^{11+} irradiations, it is not sure whether a saturation effect for amorphization could occur or not due to the absence of data at higher irradiation dose. On the one hand, the fitting formula indicates that the complete amorphization $f_a = 1$ can be achieved at extremely high irradiation dose. On the other hand, as shown in Table 1, the electronic to nuclear stopping power ratio (ENSP) Ar^{11+} ions is relatively high, which could enhance the annihilation of defects. In addition, the Ar^{11+} irradiations were also carried out at room temperature. At this point, the saturation of amorphization at $f_a < 1$ may occur in $Lu_2Ti_2O_7$ under Ar^{11+} irradiation. More data at higher irradiation doses are needed to draw a clear conclusion.

As mentioned in Section 3, lattice swelling effect is also pronouncedly induced in $Lu_2Ti_2O_7$ before amorphization by all ion irradiations. The calculated lattice swelling percentages, $\Delta a/a_0$ (a_0 is the lattice parameter of pristine $Lu_2Ti_2O_7$), are plotted in Fig. 5. The lattice parameter increases with increasing irradiation dose for each ion species. The pre-amorphization lattice swelling effect in pyrochlores induced by ion beam irradiations has been well investigated previously [25,26]. Based on the experimental observations and atomistic simulations in Ref. [25], it is easily understood that the lattice swelling induced by 400 keV Ne^{2+} irradiation in $Lu_2Ti_2O_7$ at cryogenic temperature is initially due to the formation of cation antisite defects. As irradiated at the same dose, the swelling percentage, $\Delta a/a_0$, increases significantly with increasing ion mass and energy. Similarly, we can also conclude that the heavier ions are more efficient to induce lattice swelling in $Lu_2Ti_2O_7$.

To address the discrepancy in radiation effects (amorphization and lattice swelling) of $Lu_2Ti_2O_7$ under 400 keV Ne^{2+}, 2.7 MeV Ar^{11+} and 6.5 MeV Xe^{26+} ion irradiations, we try to make a detailed and evidenced interpretation from two aspects in following sections.

4.2. Role of defect configuration

Radiation induced structural evolution in materials is generally due to the formation, accumulation, migration and clustering of defects. In $A_2B_2O_7$ pyrochlores, radiation induced defects can be

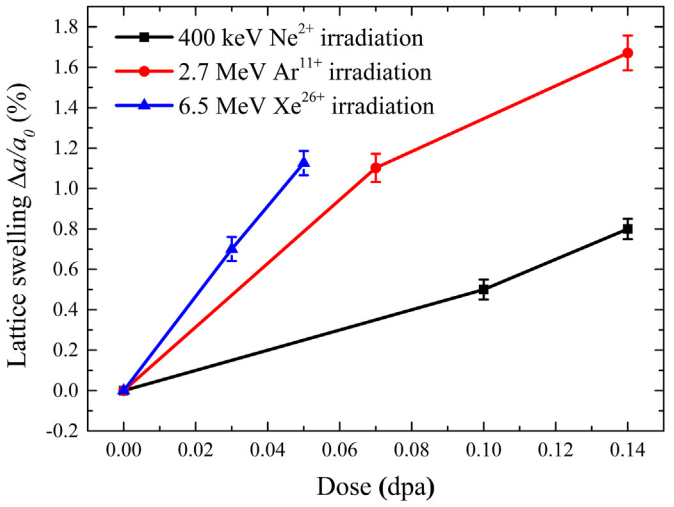

Fig. 5. Lattice swelling percentages, $\Delta a/a_0$, as a function of irradiation dose in $Lu_2Ti_2O_7$ pyrochlores before amorphization under 400 keV Ne^{2+}, 2.7 MeV Ar^{11+} and 6.5 MeV Xe^{26+} irradiation. The lattice parameter increases with increasing dose for each ion species irradiation. The increasing rate also increases with increasing ion mass and energy.

basically summarized by the following point-defect reactions:

$$A_A + B_B \rightarrow A_B + B_A, \quad (4)$$

$$A_A \rightarrow V_A + A_i, \quad (5)$$

$$B_B \rightarrow V_B + B_i, \quad (6)$$

$$O_O \rightarrow V_O + O_i. \quad (7)$$

As a result, cation antisites (A_B, B_A), interstitials (A_i, B_i, O_i) and vacancies (V_A, V_B, V_O) defects would be produced in $A_2B_2O_7$ lattice. Theoretical investigations [10,25,27–30] have demonstrated that the cation antisite defects are the most energetically favorable and stable defect type in several titanate pyrochlores and strongly correlated to their susceptibility to radiation induced amorphization. In our previous study on $Lu_2Ti_2O_7$, the formation energies for near and far cation antisites are 0.81 and 0.85 eV respectively, much lower than those of Lu (2.8 eV) and Ti (3.3 eV) Frenkel pairs [25]. Furthermore, the temperature accelerated dynamics (TAD) simulations implied that the Frenkel defects are metastable and would decay to form antisite defects [25]. It should be noted that it does not absolutely mean that only antisite defects are induced in pyrochlores under irradiations. Actually, other defect types are also introduced with a relatively small proportion. The cation antisite is also the primary cause of ion irradiation induced lattice swelling in pyrochlores [25]. From this point, assuming that the defects retained from collision cascades in $Lu_2Ti_2O_7$ under each ion irradiation consists mainly of cation antisites, the same irradiation dose should correspond to the same amount of antisites since the antisites would stably exist once formed. As a result, the same extent of amorphization and lattice swelling would be triggered. However, the extents of amorphization and lattice swelling at the same irradiation dose depend strongly on ion species from our results. Therefore, we are reasonably allowed to suppose that the defect configurations in damaged layers of $Lu_2Ti_2O_7$ are probably different under different ion irradiations. More specifically, in addition to the cation antisites, the proportion of other defect types (such as interstitials and vacancies) are also expected to increase with increasing ion mass and energy. This is reasonable because the energy of recoils increases with increasing mass and energy of implanted ions applied in this work, as shown in Table 2. These defect types also contribute partially or predominantly to the radiation behavior of $Lu_2Ti_2O_7$ pyrochlores under heavier ion irradiations. This inference is supported by two pieces of evidences. Firstly, we will discuss from the perspective of amorphization. According to *Shen* [45], a phase transition (e.g. amorphization or a change in crystallographic structure) in irradiated materials is thermodynamically possible only when

$$\Delta G_{gb} + \Delta G_{pd} > \Delta G_{pt}, \quad (8)$$

where ΔG_{gb} is the Gibbs free energy of grain boundaries, ΔG_{pd} is the Gibbs free energy of irradiation induced point defects and ΔG_{pt} is the Gibbs free energy barrier for the phase transition. In this work, all $Lu_2Ti_2O_7$ samples were synthesized through the conventional solid-state method and possess similar grain size of approximately 10 μm [43], at which the influence of grain boundary is rather weak and can be ignored. We thereby should only consider ΔG_{pd} here. As calculated previously, the defect formation energy of cation antisites is much smaller than other defect types. Accordingly, ΔG_{pd} induced by an antisite should be smaller than that induced by a defect of other types. As more other type defects are introduced, ΔG_{pd} would increases faster, and $Lu_2Ti_2O_7$ samples are thus easier to be amorphized. This is consistent with the results shown in Fig. 4(d). Secondly, Fig. 5 shows that the lattice swells more rapidly under 6.5 MeV Xe^{26+} and 2.7 MeV Ar^{11+} irradiations as compared with the case of 400 keV Ne^{2+} irradiation. It has been calculated that the formation volumes (namely, the lattice volume change induced by introducing a defect into the $Lu_2Ti_2O_7$ structure) are 49.7 and 53.5 $Å^3$ for a Lu and Ti Frenkel pair respectively, which are significantly larger than that of an antisite (~12 $Å^3$). Hence, the inclusion of other defect types can greatly enhance the lattice swelling rate of $Lu_2Ti_2O_7$, as in the cases of heavier ion irradiations.

4.3. Role of collision-cascade density

In this section, we discuss the effects of the density of collision cascades, which is alternatively responsible for the dependence of radiation behavior of $Lu_2Ti_2O_7$ on the ion species. In order to obtain the details of irradiation induced cascades, Monte Carlo simulations of the single ion implantation into $Lu_2Ti_2O_7$ has been performed using SRIM code for 400 keV Ne, 2.7 MeV Ar and 6.5 MeV Xe. The detailed collision events were presented in Table 2. The numbers of total displacements are 751, 2701 and 12255 for a single 400 keV Ne, 2.7 MeV Ar and 6.5 MeV Xe ion implantation respectively, showing a dramatic increase with increasing ion mass and energy. Fig. 6 provides the direct evidence that the displacement density of collision cascade increases following the sequence of Ne, Ar and Xe.

Table 2
The detailed collision events induced by a single ion implantation in $Lu_2Ti_2O_7$.

Ions	Maximum energy of recoils (keV)	Total displacements	Total vacancies	Replacements collisions
400 keV Ne^{2+}	1.57	751	736	15
2.7 MeV Ar^{11+}	1.92	2701	2665	36
6.5 MeV Xe^{26+}	5.57	12255	12081	174

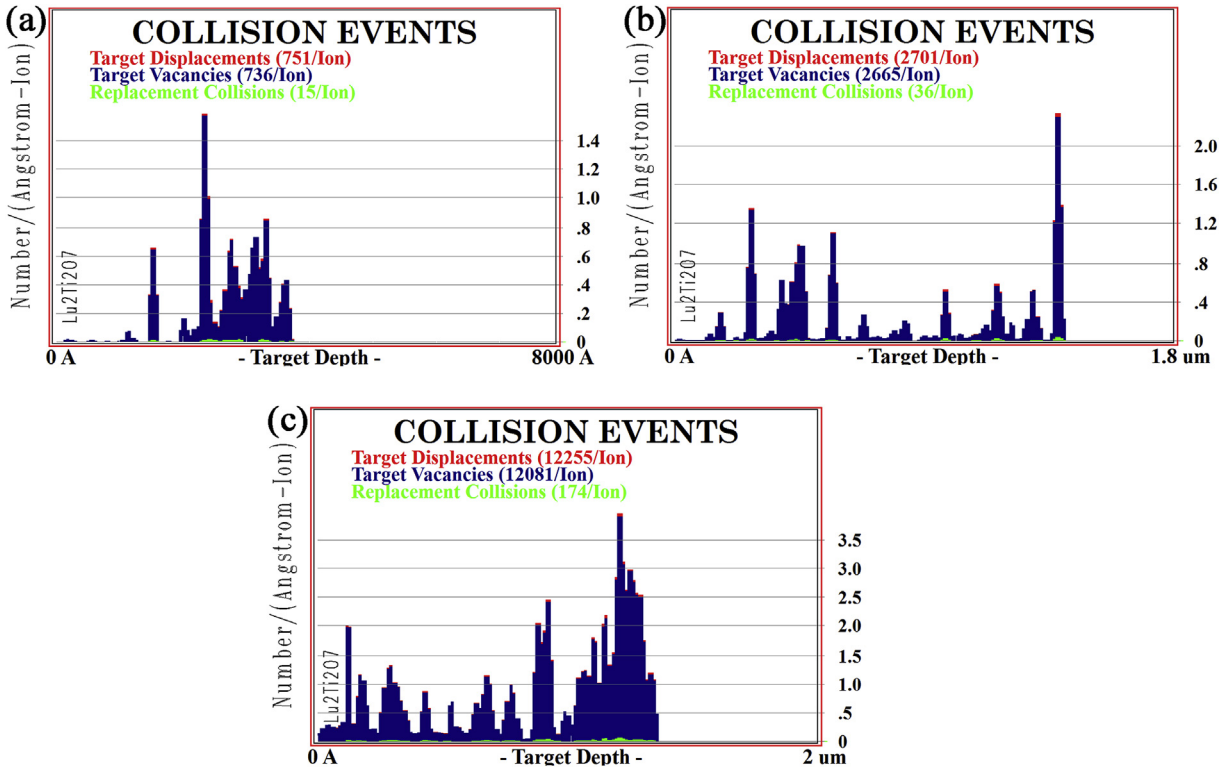

Fig. 6. The collision events in $Lu_2Ti_2O_7$ induced by a single implanted ion from SRIM simulations: (a) 400 keV Ne, (b) 2.7 MeV Ar and (c) 6.5 MeV Xe.

Generally, an increase in the density of collision cascades should enhance the clustering of mobile point defects into stable defect complexes [46]. What is more, our recent atomistic simulations (to be published elsewhere soon) have demonstrated that the defect recovery rate is much higher in the cascades initiated by a lower energy primary knock-on atom (PKA). From Table 2, the maximum energies of PKAs induced by a Ne, Ar and Xe ion are 1.57, 1.92 and 5.57 keV respectively. As a result, the defect survivability is increased under heavier ion irradiation, making $Lu_2Ti_2O_7$ prone to amorphization at a lower dose. In addition, the mass and energy-dependent damage build-up may be due to a decrease in the effective displacement energies of atoms in the $Lu_2Ti_2O_7$ matrix with increasing density of collision cascades. On the one hand, in a highly dense displacement cascade, the atomic bonds would be severely disrupted, resulting in reduced displacement energies for atoms with missing nearest neighbors [47]. On the other hand, the local structure of matrices could be distorted within the dense collision cascades [48]. With the decreased effective atomic displacement energies, the structure of materials is expected to be more susceptible to amorphization under ion irradiation.

5. Conclusions

The purpose of this work is to investigate the role of ion species in radiation effects of pyrochlores. Three ion species were separately implanted into pyrochlore $Lu_2Ti_2O_7$ samples: 400 keV Ne^{2+}, 2.7 MeV Ar^{11+} and 6.5 MeV Xe^{26+}. Both amorphization and lattice swelling are induced in $Lu_2Ti_2O_7$ under each irradiation. However, the ion species plays a significant role in the radiation effects of $Lu_2Ti_2O_7$, where heavier ions behave more efficiently to induce amorphization and lattice swelling. The threshold amorphization dose decreases with increasing ion mass and energy. Moreover, the amorphization rate, as well as lattice swelling rate, increases with increasing ion mass and energy. From the view of thermodynamics, it is supposed that the proportion of other defect types, in addition to the cation antisite, increases under heavier ion irradiations in the damaged $Lu_2Ti_2O_7$ layers, which leads to enhanced amorphization and lattice swelling rate. Alternatively, the density of collision cascades also makes a contribution. With increasing density of collision cascades, the efficiency of defect clustering into stable defect complexes is increased and the effective atomic displacement energies are reduced, both of which account for the increased susceptibility of $Lu_2Ti_2O_7$ to amorphization and lattice swelling under heavier ion irradiations. These results are much worth of consideration when accelerated ion beams are used to simulating the radiation damage induced in immobilization matrices by α- and β-decay events of radioactive wastes. This work is also expected to provide new insights into the radiation damage mechanisms of pyrochlores.

Acknowledgements

This work was sponsored by the National Natural Science Foundation of China (11475076, 11175076 and 51471160) and the Fundamental Research Funds for the Central Universities of China (Lanzhou University, lzujbky-2015-239). Ion Beam Materials Laboratory was supported by the Center for Integrated Nanotechnologies, a DOE nanoscience user facility jointly operated by Los Alamos and Sandia National Laboratories. The authors would also like to thank the operational staff at the 320 kV platform for multi-discipline research with highly charged ions at the Institute of Modern Physics, CAS.

References

[1] A.E. Ringwood, Immobilisation of high level nuclear reactor wastes in SYNROC, Nature 278 (1979) 219, http://dx.doi.org/10.1038/278219a0s.
[2] R.C. Ewing, Long-term storage of spent nuclear fuel, Nat. Mater. 14 (2015) 252–257, http://dx.doi.org/10.1038/nmat4226.

[3] L.L. Hench, D.E. Clark, J. Campbell, High level waste immobilization forms, Nucl. Chem. Waste Manag. 5 (1984) 149–173, http://dx.doi.org/10.1016/0191-815X(84)90045-7.

[4] I. Donald, B. Metcalfe, R. Taylor, The immobilization of high level radioactive wastes using ceramics and glasses, J. Mater. Sci. 2 (1997), http://dx.doi.org/10.1023/A:1018646507438.

[5] R.C. Ewing, W. Lutze, High-level nuclear waste immobilization with ceramics, Ceram. Int. 17 (1991) 287–293, http://dx.doi.org/10.1016/0272-8842(91)90024-T.

[6] R.C. Ewing, W.J. Weber, F.W. Clinard, Radiation effects in nuclear waste forms for high-level radioactive waste, Prog. Nucl. Energy 29 (1995) 63–127, http://dx.doi.org/10.1016/0149-1970(94)00016-Y.

[7] M.A. Subramanian, G. Aravamudan, G.V. Subba Rao, Oxide pyrochlores — A review, Prog. Solid State Chem. 15 (1983) 55–143, http://dx.doi.org/10.1016/0079-6786(83)90001-8.

[8] B. Mandal, A. Tyagi, Pyrochlores: Potential Multifunctional Materials, 2010. Forthcom. Issue.

[9] R.C. Ewing, W.J. Weber, J. Lian, Nuclear waste disposal-pyrochlore ($A_2B_2O_7$): nuclear waste form for the immobilization of plutonium and "minor" actinides, J. Appl. Phys. 95 (2004) 5949–5971, http://dx.doi.org/10.1063/1.1707213.

[10] J. Lian, J. Chen, L. Wang, R. Ewing, J. Farmer, L. Boatner, K. Helean, Radiation-induced amorphization of rare-earth titanate pyrochlores, Phys. Rev. B 68 (2003) 1–9, http://dx.doi.org/10.1103/PhysRevB.68.134107.

[11] M.K. Patel, V. Vijayakumar, D.K. Avasthi, S. Kailas, J.C. Pivin, V. Grover, B.P. Mandal, A.K. Tyagi, Effect of swift heavy ion irradiation in pyrochlores, Nucl. Instrum. Methods Phys. Res. Sect. B 266 (2008) 2898–2901, http://dx.doi.org/10.1016/j.nimb.2008.03.135.

[12] J. Zhang, Y.Q. Wang, M. Tang, C. Sun, D.M. Yin, N. Li, Helium irradiation induced micro-swelling and phase separation in pyrochlore $Lu_2Ti_2O_7$, Nucl. Instrum. Methods Phys. Res. Sect. B Beam Interact. Mater. Atoms 342 (2015) 179–183, http://dx.doi.org/10.1016/j.nimb.2014.09.036.

[13] J. Zhang, J. Lian, F. Zhang, J. Wang, A.F. Fuentes, R.C. Ewing, Intrinsic structural disorder and radiation response of nanocrystalline $Gd_2(Ti_{0.65}Zr_{0.35})_2O_7$ pyrochlore, J. Phys. Chem. C 114 (2010) 11810–11815, http://dx.doi.org/10.1021/jp103371j.

[14] J. Lian, R.C. Ewing, L.M. Wang, K.B. Helean, Ion-beam irradiation of $Gd_2Sn_2O_7$ and $Gd_2Hf_2O_7$ pyrochlore: bond-type effect, J. Mater. Res. 19 (2004) 1575–1580, http://dx.doi.org/10.1557/JMR.2004.0178.

[15] J. Lian, X. Zu, K. Kutty, J. Chen, L. Wang, R. Ewing, Ion-irradiation-induced amorphization of $La_2Zr_2O_7$ pyrochlore, Phys. Rev. B 66 (2002) 1–5, http://dx.doi.org/10.1103/PhysRevB.66.054108.

[16] D.M. Strachan, R.D. Scheele, E.C. Buck, A.E. Kozelisky, R.L. Sell, R.J. Elovich, W.C. Buchmiller, Radiation damage effects in candidate titanates for Pu disposition: Zirconolite, J. Nucl. Mater. 372 (2008) 16–31, http://dx.doi.org/10.1016/j.jnucmat.2007.01.278.

[17] K.E. Sickafus, J.A. Valdez, J.R. Williams, R.W. Grimes, H.T. Hawkins, Radiation induced amorphization resistance in A_2O_3-BO_2 oxides, Nucl. Instrum. Methods Phys. Res. Sect. B 191 (2002) 549–558, http://dx.doi.org/10.1016/S0168-583X(02)00609-2.

[18] K.E. Sickafus, R.W. Grimes, J.A. Valdez, A. Cleave, M. Tang, M. Ishimaru, S.M. Corish, C.R. Stanek, B.P. Uberuaga, Radiation-induced amorphization resistance and radiation tolerance in structurally related oxides, Nat. Mater 6 (2007) 217–223, http://dx.doi.org/10.1038/nmat1842.

[19] S. Park, M. Lang, C.L. Tracy, J. Zhang, F. Zhang, C. Trautmann, M.D. Rodriguez, P. Kluth, R.C. Ewing, Response of $Gd_2Ti_2O_7$ and $La_2Ti_2O_7$ to swift-heavy ion irradiation and annealing, Acta Mater. 93 (2015) 1–11, http://dx.doi.org/10.1016/j.actamat.2015.04.010.

[20] M. Lang, F. Zhang, J. Zhang, J. Wang, J. Lian, W.J. Weber, B. Schuster, C. Trasutmann, R. Neumann, R.C. Ewing, Review of $A_2B_2O_7$ pyrochlore response to irradiation and pressure, Nucl. Instrum. Methods Phys. Res. Sect. B 268 (2010) 2951–2959, http://dx.doi.org/10.1016/j.nimb.2010.05.016.

[21] M. Lang, M. Toulemonde, J. Zhang, F. Zhang, C.L. Tracy, J. Lian, Z. Wang, W.J. Weber, D. Severin, M. Bender, C. Trautmann, R.C. Ewing, Swift heavy ion track formation in $Gd_2Zr_{2-x}Ti_xO_7$ pyrochlore: effect of electronic energy loss, Nucl. Instrum. Methods Phys. Res. Sect. B 336 (2014) 102–115, http://dx.doi.org/10.1016/j.nimb.2014.06.019.

[22] M. Lang, J. Lian, J. Zhang, F. Zhang, W.J. Weber, C. Trautmann, R.C. Ewing, Single-ion tracks in $Gd_2Zr_{2-x}Ti_xO_7$ pyrochlores irradiated with swift heavy ions, Phys. Rev. B 79 (2009) 224105, http://dx.doi.org/10.1103/PhysRevB.79.224105.

[23] M. Lang, F.X. Zhang, R.C. Ewing, J. Lian, C. Trautmann, Z. Wang, Structural modifications of $Gd_2Zr_{2-x}Ti_xO_7$ pyrochlore induced by swift heavy ions: disordering and amorphization, J. Mater. Res. 24 (2009) 1322–1334, http://dx.doi.org/10.1557/jmr.2009.0151.

[24] J. Lian, L. Wang, J. Chen, K. Sun, R.C. Ewing, J.M. Farmer, L.A. Boatner, The order-disorder transition in ion-irradiated pyrochlore, Acta Mater. 51 (2003) 1493–1502, http://dx.doi.org/10.1016/S1359-6454(02)00544-X.

[25] Y.H. Li, B.P. Uberuaga, C. Jiang, S. Choudhury, J.A. Valdez, M.K. Patel, J. Won, Y.Q. Wang, M. Tang, D.J. Safarik, D.D. Byler, K.J. McClellan, I.O. Usov, T. Hartmann, G. Baldinozzi, K.E. Sickafus, Role of antisite disorder on pre-amorphization swelling in titanate pyrochlores, Phys. Rev. Lett. 108 (2012) 1–5, http://dx.doi.org/10.1103/PhysRevLett.108.195504.

[26] Y.H. Li, Y.Q. Wang, J.A. Valdez, M. Tang, K.E. Sickafus, Swelling effects in $Y_2Ti_2O_7$ pyrochlore irradiated with 400 keV Ne^{2+} ions, Nucl. Instrum. Methods Phys. Res. Sect. B 274 (2012) 182–187, http://dx.doi.org/10.1016/j.nimb.2011.11.012.

[27] H.Y. Xiao, L.M. Wang, X.T. Zu, J. Lian, R.C. Ewing, Theoretical investigation of structural, energetic and electronic properties of titanate pyrochlores, J. Phys. Condens. Matter 19 (2007) 346203, http://dx.doi.org/10.1088/0953-8984/19/34/346203.

[28] C. Jiang, C.R. Stanek, K.E. Sickafus, B.P. Uberuaga, First-principles prediction of disordering tendencies in pyrochlore oxides, Phys. Rev. B 79 (2009) 17–21, http://dx.doi.org/10.1103/PhysRevB.79.104203.

[29] H.Y. Xiao, X.T. Zu, F. Gao, W.J. Weber, First-principles study of energetic and electronic properties of $A_2Ti_2O_7$ (A = Sm, Gd, Er) pyrochlore, J. Appl. Phys. 104 (2008) 1–6, http://dx.doi.org/10.1063/1.2986156.

[30] Y. Li, P.M. Kowalski, G. Beridze, A.R. Birnie, S. Finkeldei, D. Bosbach, Defect formation energies in $A_2B_2O_7$ pyrochlores, Scr. Mater. 107 (2015) 18–21, http://dx.doi.org/10.1016/j.scriptamat.2015.05.010.

[31] G.R. Lumpkin, M. Pruneda, S. Rios, K.L. Smith, K. Trachenko, K.R. Whittle, N.J. Zaluzec, Nature of the chemical bond and prediction of radiation tolerance in pyrochlore and defect fluorite compounds, J. Solid State Chem. 180 (2007) 1512–1518, http://dx.doi.org/10.1016/j.jssc.2007.01.028.

[32] K.B. Helean, S.V. Ushakov, C.E. Brown, A. Navrotsky, J. Lian, R.C. Ewing, J.M. Farmer, L.A. Boatner, Formation enthalpies of rare earth titanate pyrochlores, J. Solid State Chem. 177 (2004) 1858–1866, http://dx.doi.org/10.1016/j.jssc.2004.01.009.

[33] R. Devanathan, W.J. Weber, J.D. Gale, Radiation tolerance of ceramics—insights from atomistic simulation of damage accumulation in pyrochlores, Energy Environ. Sci. 3 (2010) 1551, http://dx.doi.org/10.1039/c0ee00066c.

[34] L. Thomé, S. Moll, A. Debelle, F. Garrido, G. Sattonnay, J. Jagielski, Radiation effects in nuclear ceramics, Adv. Mater. Sci. Eng. 2012 (2012), http://dx.doi.org/10.1155/2012/905474.

[35] S.X. Wang, L.M. Wang, R.C. Ewing, Irradiation-induced amorphization: effects of temperature, ion mass, cascade size, and dose rate, Phys. Rev. B 63 (2000) 024105, http://dx.doi.org/10.1103/PhysRevB.63.024105.

[36] W.J. Weber, Y. Zhang, L. Wang, Review of dynamic recovery effects on ion irradiation damage in ionic-covalent materials, Nucl. Instrum. Methods Phys. Res. Sect. B 277 (2012) 1–5, http://dx.doi.org/10.1016/j.nimb.2011.12.043.

[37] J.F. Ziegler, J.P. Biersack, The stopping and range of ions in matter, in: Treatise Heavy-ion Sci, Springer US, Boston, MA, 1985, pp. 93–129, http://dx.doi.org/10.1007/978-1-4615-8103-1_3.

[38] R. Devanathan, W.J. Weber, Insights into the radiation response of pyrochlores from calculations of threshold displacement events, J. Appl. Phys. 98 (2005) 7–10, http://dx.doi.org/10.1063/1.2120889.

[39] W.J. Weber, Models and mechanisms of irradiation-induced amorphization in ceramics, Nucl. Instrum. Methods Phys. Res. Sect. B 166–167 (2000) 98–106, http://dx.doi.org/10.1016/S0168-583X(99)00643-6.

[40] D.Y. Yang, C.G. Liu, K.Q. Zhang, Y. Xia, L.J. Chen, H. Liu, Y.H. Li, 2.7 MeV Ar^{11+} ion irradiation induced structural evolution in $Lu_2(Ti_{2-x}Lu_x)O_{7-x/2}$ pyrochlores, J. Nucl. Mater. 466 (2015) 496–501, http://dx.doi.org/10.1016/j.jnucmat.2015.08.034.

[41] N. Sellami, G. Sattonnay, C. Grygiel, I. Monnet, A. Debelle, C. Legros, D. Menut, S. Miro, P. Simon, J.L. Bechade, L. Thomé, Modifications of structural and physical properties induced by swift heavy ions in $Gd_2Ti_2O_7$ and $Y_2Ti_2O_7$ pyrochlores, Nucl. Instrum. Methods Phys. Res. Sect. B 365 (2015) 371–375, http://dx.doi.org/10.1016/j.nimb.2015.07.017.

[42] X. Qiu-rong, Z. Jian, Y. Dong-min, Krypton ion irradiation-induced amorphization and nano-crystal formation in pyrochlore $Lu_2Ti_2O_7$ at room temperature, Chin. Phys. B 24 (2015) 1–5, http://dx.doi.org/10.1088/1674-1056/24/12/126103.

[43] J. Wen, C. Sun, P.P. Dholabhai, Y. Xia, M. Tang, D. Chen, D.Y. Yang, Y.H. Li, B.P. Uberuaga, Y.Q. Wang, Temperature dependence of the radiation tolerance of nanocrystalline pyrochlores $A_2Ti_2O_7$ (A = Gd, Ho and Lu), Acta Mater. 110 (2016) 175–184, http://dx.doi.org/10.1016/j.actamat.2016.03.025.

[44] E. Zarkadoula, M. Toulemonde, W.J. Weber, Additive effects of electronic and nuclear energy losses in irradiation-induced amorphization of zircon, Appl. Phys. Lett. 107 (2015), http://dx.doi.org/10.1063/1.4939110.

[45] T.D. Shen, Radiation tolerance in a nanostructure: is smaller better? Nucl. Instrum. Methods Phys. Res. Sect. B 266 (2008) 921–925, http://dx.doi.org/10.1016/j.nimb.2008.01.039.

[46] S.O. Kucheyev, J.S. Williams, C. Jagadish, J. Zou, G. Li, A.I. Titov, Effect of ion species on the accumulation of ion-beam damage in GaN, Phys. Rev. B 64 (2001) 035202, http://dx.doi.org/10.1103/PhysRevB.64.035202.

[47] J.S. Williams, Ion implantation of semiconductors, Mater. Sci. Eng. A 253 (1998) 8–15, http://dx.doi.org/10.1016/S0921-5093(98)00705-9.

[48] S.O. Kucheyev, J.S. Williams, C. Jagadish, J. Zou, G. Li, Damage buildup in GaN under ion bombardment, Phys. Rev. B 62 (2000) 7510–7522, http://dx.doi.org/10.1103/PhysRevB.62.7510.